ELSEVIER

NeuroImage

www.elsevier.com/locate/ynimg
NeuroImage 34 (2007) 85–93

Shape variability of the human striatum—Effects of age and gender

Juha Koikkalainen,[a,c,*] Jussi Hirvonen,[b] Mikko Nyman,[b] Jyrki Lötjönen,[c] Jarmo Hietala,[b,e] and Ulla Ruotsalainen[d]

[a]*Laboratory of Biomedical Engineering, Helsinki University of Technology, P.O. Box 2200, FIN-02015 HUT, Finland*
[b]*Turku PET Centre, P.O. Box 52, FIN-20521 Turku, Finland*
[c]*VTT Technical Research Centre of Finland, P.O. Box 1300, FIN-33101 Tampere, Finland*
[d]*Institute of Signal Processing, Tampere University of Technology, P.O. Box 553, FIN-33101 Tampere, Finland*
[e]*Department of Psychiatry, University of Turku, FIN-20700 Turku, Finland*

Received 24 March 2006; revised 9 August 2006; accepted 13 August 2006
Available online 23 October 2006

Human striatum is involved in the regulation of movement, reinforcement, learning, reward, cognitive functioning, and addiction. Previous classical volumetric MRI studies have implicated age-, disease- and medication-related changes in striatal structures. Yet, no studies to date have addressed the effects of these factors on the shape variability and local structural alterations in the striatum. The local alterations may provide meaningful additional information in the context of functional neuroanatomy and brain connectivity. We developed image analysis methodology for the measurement of the volume and local shape variability of the human striatum. The method was applied in a group of 43 healthy controls to study the effects of age and gender on striatal shape variability. In the volume analysis, the volume of the striatum was normalized using the volume of the whole brain. In the local shape analysis, the deviations from a mean surface were studied for each surface point using high-dimensional mapping. Also, discriminant functions were constructed from a statistical shape model. The accuracy and reproducibility of the methods used were evaluated. The results confirmed that the volume of the striatum decreases as a function of age. However, the volume decrease was not uniform and age-related shape differences were observed in several subregions of the human striatum whereas no local gender differences were seen. Examination of the variability of striatal shape in the healthy population will pave the way for applying this method in clinical settings. This method will be particularly useful for investigating neuropsychiatric disorders that are associated with subtle morphological alterations of the brain, such as schizophrenia.

Introduction

Human striatum is a group of nuclei in the brain, which can be structurally divided into the caudate nucleus, putamen, and nucleus accumbens. Striatum receives afferent input from the cortex, and sends projections back to the cortex via thalamus. Different parts of the striatum receive input from different cortical regions, which serves as the basis of the functional division of the striatum into limbic, associative, and sensorimotor parts (Parent and Hazrati, 1995; Haber, 2003). Via these functional cortico-striato-thalamo-cortical neural networks, the striatum is involved in various brain functions, such as regulation of motor control, learning, reward, cognitive functioning, and addiction. Variability in local structure of the striatum in health and disease could thus be related to many clinical phenomena, such as age-related decline in motor and cognitive functions, and known gender differences in cognition (Rilea et al., 2004; Guillem and Mograss, 2005) and also in prevalence of various psychiatric diseases.

The progress in brain atlases and high-dimensional mapping has enabled the accurate local computational analysis of the brain structures (Thompson and Toga, 2002). These methods enable quantification, statistical analysis, and visualization of local structural changes. The simplest possibility to study the brain structures is to analyze the volumes of the objects of interest. Previously, the effects of aging (Gunning-Dixon et al., 1998; Xu et al., 2000; Gunduz et al., 2002; Gur et al., 2002; Brabec et al., 2003) and disease (Shihabuddin et al., 2001; Strakowski et al., 2002; Gunduz et al., 2002; Levitt et al., 2002; Lacerda et al., 2003; Buchsbaum et al., 2003; Aylward et al., 2004; Deshmukh et al., 2005; Hollander et al., 2005) in the volume of the striatum have been studied. However, shape could provide additional and complimentary information about local structural alterations meaningful in the context of functional neuroanatomy. First, two structures with equal volumes might have completely different shapes. Second, local shape variation does not necessary result in a detectable volume change and shape analysis could thus be more sensitive to subtle alterations. Third, contrary to volume analysis, shape analysis provides a detailed localization of structural changes. Therefore, more detailed shape analysis is needed for more accurate understanding of the human brain connectivity (Csernansky et al., 1998; Tepest et al., 2003; Posener et al., 2003; Behrens et al., 2003; Styner

* Corresponding author. Juha Koikkalainen, VTT Technical Research Centre of Finland, P.O. Box 1300, FIN-33101 Tampere, Finland. Fax: +358 20 722 3380.
E-mail address: juha.koikkalainen@vtt.fi (J. Koikkalainen).
Available online on ScienceDirect (www.sciencedirect.com).

1053-8119/$ - see front matter © 2006 Elsevier Inc. All rights reserved.
doi:10.1016/j.neuroimage.2006.08.039

et al., 2005). However, the shapes of individual brain structures are very difficult to analyze visually since many diseases, gender, and aging may cause small local changes in brain anatomy, and the normality of the individual brain and local structural changes have to be analyzed by studying the variability among a group of individuals. So far, the shape of the striatum has been studied in clinical settings in only two published papers (Levitt et al., 2004; Hwang et al., 2006). Therefore, it is important to study the age- and gender-related shape changes of the striatum in healthy individuals.

Detailed shape analysis of a brain structure is done by utilizing the correspondence between the shape representations of individuals. The structure is segmented and the correspondence is established. This is most often done using high-dimensional mapping (Christensen et al., 1997; Davatzikos, 1997; Bookstein, 1997; Thompson and Toga, 2002; Csernansky et al., 2004). After the correspondence has been found, the shapes of the control and study groups can be compared, and the statistically significant group differences identified. The signed distances between the study shape and the template or the subject pair shape were utilized in (Lee et al., 2004; Styner et al., 2004, 2005; Golland et al., 2005). Another option is to compare the deformation fields of the high-dimensional mappings needed to spatially normalize the shapes for the establishment of the correspondence. In (Csernansky et al., 1998; Tepest et al., 2003), the dimensionality of the problem was reduced by applying the principal component analysis (PCA) to the deformation fields, and a linear discriminant function was created for the control and study groups using the largest eigenfunctions. In (Levitt et al., 2004), a shape index that measured the sphericity showed differences in the shape of the caudate nucleus between schizophrenic and healthy subjects. Sampath et al. (2003) used medial representation to study shape differences in schizophrenia, and Hwang et al. (2006) detected striatal shape changes in patients with bipolar disorder using spherical harmonic description.

In the study described in this paper, the shape of the striatum was studied from magnetic resonance (MR) images of healthy male or female volunteers. The objective was to examine the shape changes in aging and between genders, and to quantify, statistically analyze, and visualize them. Both volume and local shape changes were analyzed. We used a fully 3D manual segmentation software to accurately extract the shape of the striatum from the MR volume images. The shape was described using a triangular surface. Then, modern registration methods were used to register the sample surfaces. The shape analysis was based on the deformation fields from the surface representing the mean of the sample surfaces to each sample surface. Local shape differences were studied using sample surfaces' surface points' projections to the normal vectors of the mean surface. Discriminant functions were constructed using a statistical shape model.

Materials

The study was performed in accordance with the Declaration of Helsinki. All participants gave written informed consent prior

Fig. 1. An example of the MR images, and the software tool used for the manual segmentations.

inclusion to the study. 43 healthy volunteers (33 male and 10 female, mean age 29.2 ± 10.2 years, age range 19–55 years) with no history of somatic illness, head injury, drug abuse, or psychiatric disorders were studied. They were all screened by a physician to exclude any clinically significant physical abnormalities and their blood and urine laboratory tests were normal. Blood and urine drug screens were negative. Subjects were scanned with 1.5 T MRI (Siemens Magnetom, Iselin). The size of the images was $256 \times 256 \times 128$, and the resolution was either $1.5 \times 1.5 \times 1.5$ mm^3 or $1.1 \times 1.1 \times 1.5$ mm^3. Different image resolutions did not affect the analysis in any way since the shape of the striatum could be determined with an adequate accuracy from all the images. An example of the MR images, which is zoomed to the region of interest, is shown in Fig. 1.

Methods

Manual segmentation

It is important to be able to accurately determine the shape of the striatum from the MR volume images in order to detect and analyze subtle shape variations. In this study, the striatum was manually segmented from each MR image using a 3D software tool, designed for interactively making 3D deformations (Fig. 1) (Lötjönen, 2003). With the tool, a triangulated surface model (white contours superimposed on the MR images in Fig. 1) was registered manually and non-rigidly to the edges in the target MR image. The user could drag-and-drop the surface locally in 3D. The surface was elastically deformed inside a box of interest (the white 3D box on the MR images in Fig. 1): the deformation was zero on the borders and outside the box, and as dragged by the user in the center of the box. User could define the size and location of the box. The tool showed three cross-sections of the volume and the deformations could be made in any of these cross-sections. Simultaneous use of three cross-sections improves the segmentation accuracy particularly in the regions where the contrast between objects is weak in one or more cross-sections. In addition to the elastic deformation, the surface could be translated, rotated, and scaled.

All the segmentations were done by the same observer during four consecutive days. As a result, the surfaces that represented the striatum were obtained for each subject. The surfaces were represented as triangular surfaces. An example of the surfaces is shown in Fig. 2.

Volume analysis

From the manual segmentations, the volume of the striatum was defined as the volume inside the surface. To co-variate the volume of the striatum with the size of the whole brain, the volume of the brain was determined by manually segmenting it from the MR images using the software tool presented in Manual segmentation. The normalized volume of the striatum was defined by dividing the volume of the striatum by the volume of the whole brain:

$$V_{\text{striatum,normalized}} = \frac{V_{\text{striatum}}}{V_{\text{brain}}} 100. \quad (1)$$

The relations between volumes and age were studied using linear regression analysis ($p < 0.05$).

Construction of the spatial correspondence

In the shape analysis methods used in this study, the spatial correspondence between the sample subjects has to be known. In practice, we established the correspondence between the surface points (i.e., for each node of triangular surfaces) by registering the sample surfaces. The flowchart for the construction of the spatial correspondence and the surfaces for the shape analysis is shown in Fig. 3.

First, binary images were constructed from the surfaces. In the binary images, the volume inside the surface was represented using the gray-level value one, and the rest of the images was represented using the value zero. The binary images were generated in the resolution of $0.5 \times 0.5 \times 0.5$ mm^3. The higher resolution than the resolution of the original MR volume images was used to produce a smooth representation of the surfaces.

To find the correspondence between the surface points, one sample subject was randomly selected as a reference subject, and the binary images of the remaining sample subjects were aligned with the binary image of the reference subject using nine-parameter affine transformation (translation, rotation, and anisotropic scaling). The transformation parameters were optimized by minimizing the mean of the absolute values of the gray-scale differences between the two images using gradient optimization (see, for example, Press et al. (1992)). For binary images, the minimization of gray-scale differences corresponds to the maximization of the number of identical classifications in the two images. After this, the surface of the reference subject was non-rigidly registered to each aligned sample surface using a method based on free-form deformation

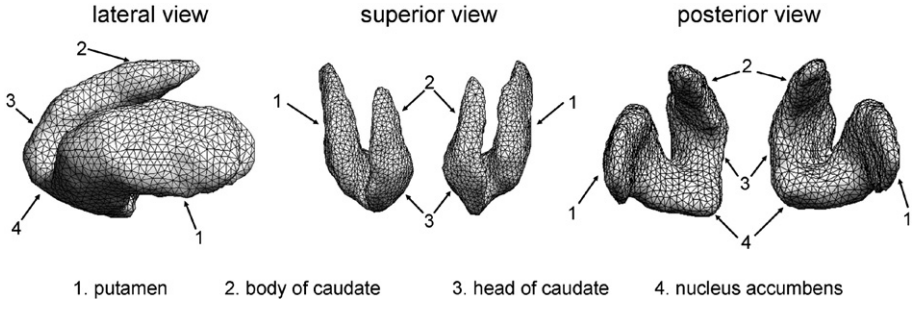

Fig. 2. Visualization of the structural parts of the striatum (caudate nucleus, putamen, and nucleus accumbens) of one sample subject using three orthogonal views. Tail of caudate could not be segmented due to resolution reasons. The surfaces visualized were obtained from manual segmentations and were represented using triangular surfaces (in total 2987 nodes and 5966 triangles).

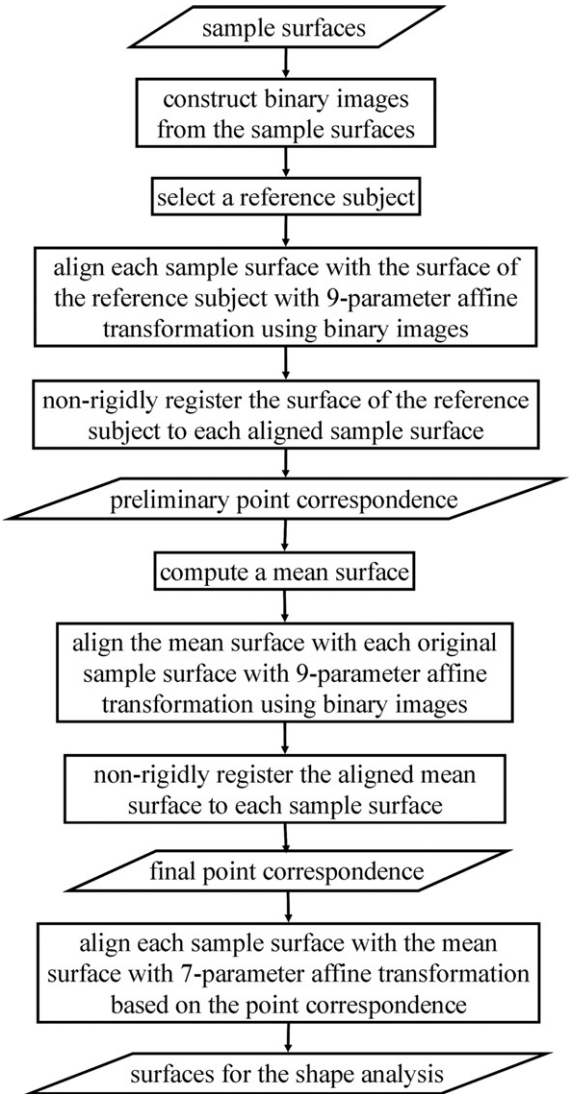

Fig. 3. A flowchart for the construction of the spatial correspondence and the surfaces for the shape analysis.

(FFD) (Lötjönen et al., 1999). In FFD (Sederberg and Parry, 1986; Lötjönen et al., 1999; Rueckert et al., 1999), the deformation of the surface was implemented using a regular grid of control points that surrounded the surface of the reference subject. The deformation was obtained by interpolating the displacements of the control points using a polynomial basis function. The control point locations were optimized by minimizing the distance from the surface of the reference subject to the sample surface. The distance was computed using six oriented distance maps determined for the sample surface (Lötjönen et al., 1999). The grid size was iteratively increased from $3\times3\times3$ to $20\times20\times20$ during the registration to have a global-to-local approach. The registrations using FFD produced representations of each sample subject's surface with the same number of surface points, and the same point represented the same anatomical feature in each surface. A mean surface $\bar{s}$ was constructed from these surfaces by averaging the representations:

$$\bar{s} = \frac{1}{N}\sum_{i=1}^{N} s_i, \tag{2}$$

where N was the sample size and s_i the representation of the surface of the ith sample subject (i.e., the surface point locations).

To reduce the bias towards the selected reference subject and to guarantee accurate point correspondence, the obtained mean surface was used as the reference, and the registration methods described above were used to register the mean surface to each original sample surface using first nine-parameter affine transformation and then non-rigid registration. The results of the registrations, the deformed mean surfaces, were then used as the representations of the sample surfaces. Finally, each sample surface was aligned with the mean surface using seven-parameter affine transformation. The alignments were done by minimizing the mean squared distance between the corresponding surface points of the mean surface and the sample surfaces using the method proposed by Arun et al. (1987). After this, all the sample surfaces were represented using the same number of surface points for which the point correspondence existed, and the pose differences were removed from the data. Finally, a new mean surface $\bar{s}$ was computed from the aligned sample surfaces using Eq. (2). Since the seven-parameter affine transformation included isotropic scaling, the size differences were removed from the data and the shape analysis was focused on the real shape variations.

Shape analysis

Two approaches were used to study the age- and gender-related shape differences. (1) The spatial deviations from the mean surface were studied for each surface point and statistical tests were performed to locate the areas where statistically significant shape variations existed (Statistical analysis of local shape differences). (2) A statistical shape model was used to generate such discriminant function that strongly correlated with the age or gender (Discriminant function). The discriminant function was used to study and visualize the global shape difference patterns. It could also be used to classify the striatal shapes of individuals to normal or abnormal.

Statistical analysis of local shape differences

For the local shape analysis, the surface normal vector, the vector perpendicular to the surface, was determined for the mean surface in each surface point. Then, for each surface point i and for each sample subject j, the difference vector from the mean surface point, $\vec{s}_i$, to the subject surface point, $\vec{s}_{i,j}$, was calculated,

$$\vec{d}_{i,j} = \vec{s}_{i,j} - \vec{s}_i, \tag{3}$$

and the difference vector was projected on the normal vector,

$$f_{i,j}^{(1)} = \vec{d}_{i,j}^{\,T}\vec{n}_i, \tag{4}$$

where $\vec{n}_i$ was the normal of the mean surface. The value $f_{i,j}^{(1)}$ was large positive if the difference vector from the mean surface to the sample surface pointed to the same direction as the normal vector, and large negative if it pointed to the opposite direction.

Statistically significant age-related local shape changes were detected by applying linear regression analysis ($p<0.05$) to the values $f_{i,j}^{(1)}$ and age, separately for each surface point. For the gender-related shape changes, one-way ANOVA ($p< 0.05$) was used. As the number of tests was several thousands, the p-value had to be corrected for the multiple comparisons. In this study, we used the Bonferroni adjustment. The corrected p-value was computed using the SISA (Simple Interactive Statistical Analysis)

software (Uitenbroek, 1997), in which the p-value was adjusted based on the number of tests and the mean correlation of the data between each surface point.

Discriminant function

To construct discriminant functions, methods related to the ones presented in (Csernansky et al., 1998; Tepest et al., 2003) were used. The objective was to construct such modes of shape variation that explained the gender and age variations as accurately as possible.

The mode of shape variation is a global representation of shape variations. It gives for each surface point a deformation vector from the mean surface. A scalar value, which can be used in the discrimination, is obtained by projecting the sample surface's deviation from the mean surface to the mode of shape variation.

The modes of shape variation were generated using a point distribution model (PDM) (Cootes et al., 1995). In the PDM, a set of orthogonal and un-correlated modes is generated so that the first t modes explain maximal amount of the variance in data. In practice, the mean and covariance matrix,

$$\Sigma = \frac{1}{N-1}\sum_{i=1}^{N}(s_i - \bar{s})(s_i - \bar{s})^T, \quad (5)$$

of the data are constructed. The eigenvectors of the covariance matrix, $\Phi=[\varphi_1,\ldots,\varphi_t]$, are the modes of shape variation and the corresponding eigenvalues give the amount of the variance in the data that the modes explain.

With the PDM modes of shape variation, a set of feature values for each sample surface were obtained from

$$f_i^{(2)} = \Phi^T(s_i - \bar{s}). \quad (6)$$

To produce a mode which explained more accurately the age and gender-related shape differences the PDM modes obtained were combined. The optimal set of modes was searched using regression analysis, and the optimal weights b_{reg} for the linear combination of the modes were computed. A new feature was obtained by combining the original feature values:

$$f_i^{(3)} = b_{\mathrm{reg}}^T f_i^{(2)} \quad (7)$$

The capability of the discrimination functions obtained to explain the age-related shape changes and to separate the genders were analyzed using correlation analysis and one-way ANOVA ($p<0.05$), respectively. The global shape difference patterns could be visualized by plotting the mean surface and the mean surface deformed according to the best modes of shape variation on top of each other. This revealed the locations where the differences existed and showed the direction and magnitude of the shape changes.

Evaluation of the methods used

The procedure presented above contained many steps which were potential error sources and might skew the results. Therefore, we performed detailed evaluation of the procedure and evaluated different error sources.

The first step was the manual segmentation of the striatum from the MR images. To evaluate the accuracy and especially the reproducibility, another observer segmented 11 cases anew. The segmentations of two observers were compared by computing the distances between the segmentations. This produced the mean error of 0.84 mm. In other words, sub-voxel accuracy was obtained. The statistics of this error source are available in Table 1.

Table 1
The statistics from the evaluation of the error sources (mm)

	Manual segmentation	Registration	Point correspondence
Minimum	0.00	0.00	0.0043
Mean	0.84	0.11	0.49
Median	0.70	0.089	0.42
Maximum	5.65	2.03	7.14
Standard deviation	0.68	0.096	0.34

The statistics are computed over all the surfaces and all the surface points.

The second error source was the non-rigid registration of the mean surface to the sample surface in the spatial normalization of the sample subjects. If the registration had been inaccurate, the analysis would have been applied to erroneous surfaces and, therefore, the real shape variability would not have been studied. The accuracy of non-rigid registrations was evaluated by determining the distances from the registration results to the surfaces of the manual segmentations. The statistics of these errors are shown in Table 1.

The accuracy of the point correspondence was evaluated by generating 50 synthetic surfaces using the PDM constructed from the sample surfaces. This guaranteed that the synthetic surfaces were realistic and that the necessary information on the point locations was available. The mean surface was deformed by randomly generating weights for the PDM modes from the normal distribution $N(0, 1)$. In addition, random affine transformation was applied to the synthetic surfaces. The transformation parameters were generated from the normal distributions as follows: translation $N(0, 2.5)$ mm, rotation $N(0, 0.1)$ rad, and scaling $N(1, \frac{1}{3})$. The same procedure that was used to establish the point correspondence for the real data was used to register the mean surface to the synthetic surfaces. The registration errors and the errors in the point correspondence were calculated from the registrations. The registration errors were very close to the errors obtained for the registration of the real data. For example, the mean error was 0.092 mm for the synthetic data whereas it was 0.11 mm for the real data. Visual examination proved that the synthetic shapes were realistic, too. The point correspondence errors were calculated as the distances between the corresponding points in the original synthetic surfaces and the surfaces obtained with the automatic registration. The error statistics are shown in Table 1.

Results

Volume analysis

The original and normalized striatum volumes are plotted as a function of age in Fig. 4. The correlation coefficient between the original volume and age was $c=-0.51$, and between the normalized volume and age $c=-0.43$. In linear regression analysis, both the total brain volume ($p< 0.0005$) and the age ($p< 0.005$) were statistically significant predictors of the striatal volume.

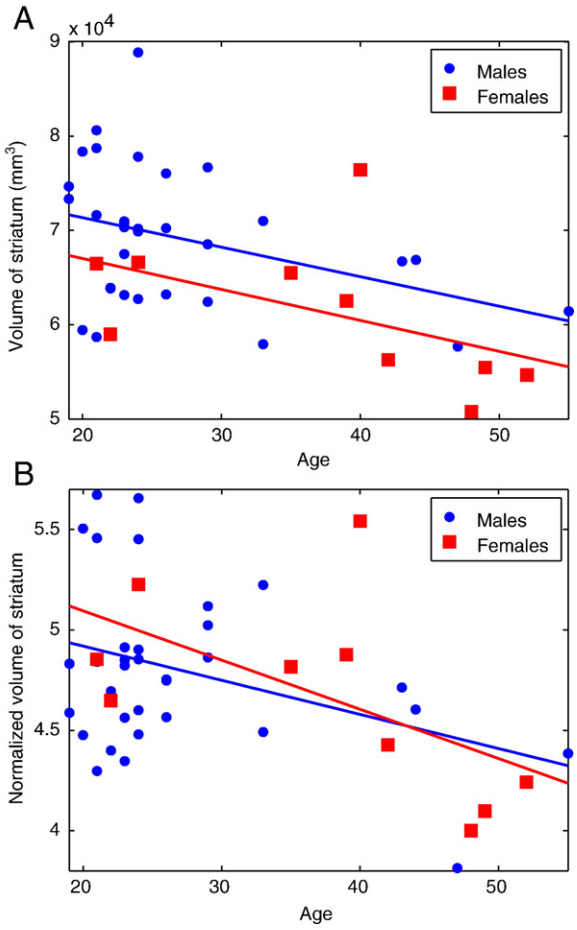

Fig. 4. (A) The correlation between the volume of the striatum and age ($c=-0.51$). (B) The correlation between the normalized volume of the striatum and age ($c=-0.43$). Linear regression curves are plotted for males and females, too.

Linear regression curves are plotted in Fig. 4 for both males and females. There were no statistically significant differences in the parameters of the regression curves, neither for the original nor for the normalized volumes. The estimated volume reduction rate for the males was 4.5% per decade for the original volumes and 3.5% per decade for the normalized volumes. The corresponding figures for the females were 5.3% and 5.3%.

Shape analysis

The modes of shape variation were constructed using leave-one-out cross-validation. In other words, the data of one sample subject was regarded as the new data that have to be analyzed, and the remaining subjects were used to construct the mean surface, the PDM modes, and the regression model of the PDM modes. This was repeated for each sample subject, and the results were combined to evaluate the methods.

Gender-related shape changes

The statistical analysis showed that there were no statistically significant local shape differences between males and females. However, global shape differences were observed: both the best PDM mode and the regression mode were able to statistically significantly discriminate genders ($p<0.01$). The correlation between the discrimination function value and gender was $c=0.40$ for the best PDM mode and $c=0.60$ for the linear combination of four PDM modes.

Age-related shape changes

The results of the statistical analysis on local age-related shape changes are shown in Fig. 5. The character of the local shape differences can be perceived from Fig. 6 in which the mean surfaces of the sample subjects younger and older than the mean of the age range (37 years) are visualized on top of each other. Age-related shape differences can be seen mostly in the head of caudate and anterior putamen.

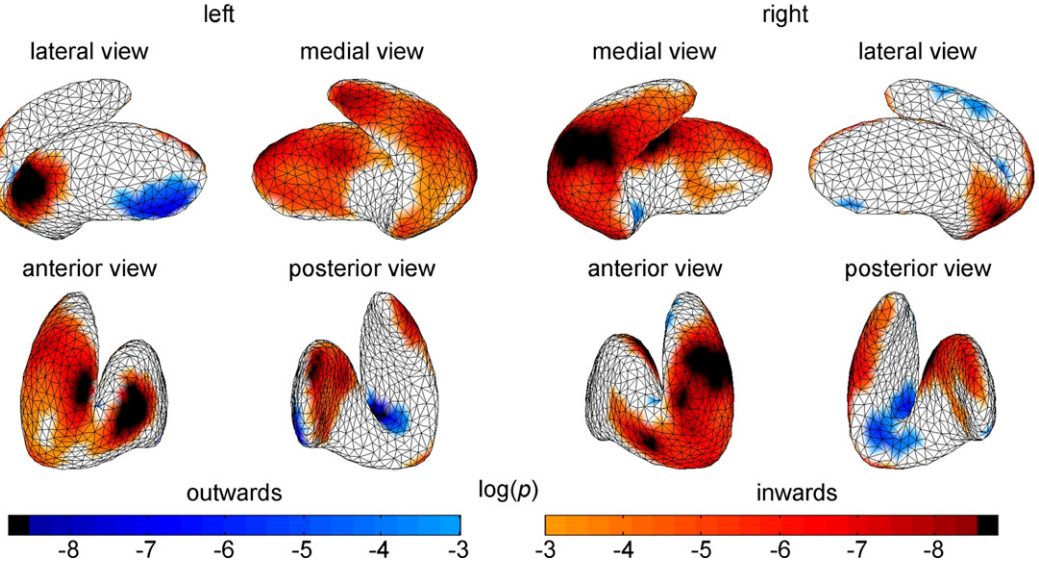

Fig. 5. The p-values of the statistical tests of the local shape changes in aging. The images show the logarithm of the p-values. The inwards deformation of the surface of the striatum in aging is represented in red colors, and the outwards deformation in blue colors. The locations where statistically significant shape changes were detected are shown in black color. The p-values larger than 0.05 are shown in white in the images.

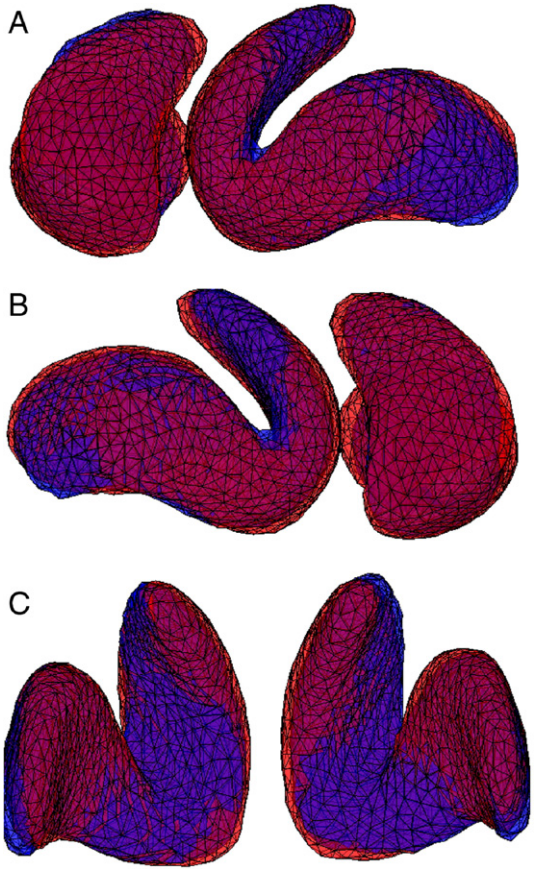

Fig. 6. The mean surfaces of the subjects younger and older than the mean of the age range (37 years) visualized on top of each other. The red surface represents the group of younger people and the blue surface represents the group of older people.

The first PDM mode of shape variation gave the best correlation with age ($c=0.60$). The correlation was improved by combining the modes using regression analysis. The combination of six modes gave the correlation of $c=0.75$. Both correlations were statistically significant ($p<0.01$). The relation between the regression mode and age is visualized in Fig. 7.

Discussion

In the studies presented in this paper, we have developed a method for the assessment of striatal shape in healthy human volunteers. We have examined the contributions of age and gender to the variation of the striatal shape measures. The applied methodology is relatively novel, since methods used to investigate striatal shape have been used in clinical settings in only two published papers (Levitt et al., 2004; Hwang et al., 2006). Thus, defining the age- and gender-related variability in the striatal shape measures in the healthy human population is crucial before this method is applied in clinical patient populations more widely.

The volume analysis showed that the volume of the striatum decreases as a function of age. Statistically significant volume decrease was observed also when the volume was normalized by the volume of the whole brain. This age-related decline in the striatal volume is in good concordance with previous reports (Gunduz et al., 2002; Gunning-Dixon et al., 1998; Xu et al., 2000; Gur et al., 2002; Brabec et al., 2003). Lack of statistically significant age by gender interactions implied that the age-related decline is similar in males and females. However, Fig. 4b suggested that the decline is steeper in females. Previous studies have shown steeper decline in females than males (Brickman et al., 2003), or vice versa (Xu et al., 2000), or no differences between genders (Gunning-Dixon et al., 1998; Gur et al., 2002; Brabec et al., 2003).

A statistically non-significant trend was noted towards males having larger striatal volume compared with females, but this trend disappeared when normalized volumes were used. Previously, women have been reported to have larger standardized basal ganglia volumes compared with men in some studies (Xu et al., 2000; Szabo et al., 2003). Clearly, the current sample size is not optimal in terms of statistical power to detect gender differences in striatal volume or in age-related decline in striatal volume: if more subjects had been studied, the results would have became more reliable and the differences observed in Fig. 4 would probably have been statistically significant.

In the shape analysis, it was first studied if there were shape differences between genders. No such surface points for which statistically significant shape differences existed were found. As there were no gender-related local shape differences, gender could be left outside the analysis when the age-related shape changes were studied.

Local statistically significant shape changes in aging were observed in several regions, mostly anterior putamen and the head of caudate, bilaterally. On the right side, the shape change extended into the ventral striatum. In these areas, the surface tended to be less convex following aging, and these changes were viewed as representing local shrinkage of the striatum. The analysis using the modes of shape variation showed similar results. The modes, especially the regression PCA mode, correlated relatively strongly with age.

Some limitations and sources of error must be considered. First, the applied MR instrumentation sets limitations with regard to spatial resolution. For example, the tail of caudate cannot be fully extracted with certainty from these MR images (Fig. 2). Second, the striata were segmented manually. This was used as automatic segmentation methods may produce large errors and still require visual inspection. Therefore, as the sample size was relatively

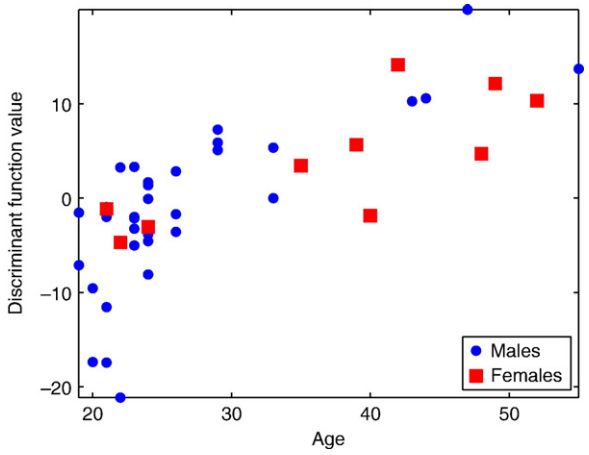

Fig. 7. The relation between the feature obtained from the regression PDM mode and age. The correlation coefficient was $c=0.75$.

small, the manual segmentation was considered to give more accurate and reliable results with a moderate workload. In the future, as the number of subjects increases and clinical applications are launched, automatic segmentation methods are necessary and have to be validated. The reproducibility of the manual segmentation was good, and the differences between the two observers were smaller than the voxel dimensions. Third, registration error could theoretically bias the current results. However, the registration accuracy was very good, and the errors in the point correspondence were small. The distributions of the errors were examined: when the distributions of each error source and the maps of the statistical analyses were compared, it turned out that the statistically significant shape differences were on the locations where the errors in each step were small. Thus, the analysis was accurate in these regions, and the results obtained were reliable. If the errors had been as small everywhere, new locations with statistically significant shape differences could have been found. This aspect should be evaluated in the future studies. Finally, the sample size was relatively small and the negative result from the gender analysis is vulnerable to type II error. The age distribution was also skewed and the gender distribution was unbalanced. Future studies should consider including more older people (over 50 years) and females in the analysis for more accurate and reliable volume and shape analysis.

A tripartite functional segregation of the striatum into limbic (nucleus accumbens, and ventral parts of caudate and pre-commissural putamen), associative (most of the head of caudate and ventral parts of pre-commissural putamen), and sensorimotor (post-commissural putamen) (Parent and Hazrati, 1995; Haber, 2003) division provides a general framework within which to interpret the current results. Shape changes observed in the current study were located mostly in the head of caudate and anterior putamen. Thus, the observed age-related shape changes seem to localize in the associative striatum. The head of caudate is involved in cognitive functioning because it receives heavy afferent innervation from the prefrontal cortex, a brain region involved in cognition (Parent and Hazrati, 1995; Goldman-Rakic, 1996; Levy et al., 1997; Manoach et al., 2000). Thus, the observed shape changes may be related to age-related decline in cognitive capabilities: among other cognitive domains, working memory performance declines with increasing age and this impairment is likely to be associated with functional and morphological changes in the neural circuits that support working memory (Grady, 2000; Burke and Barnes, 2006). Although motor skills decline with aging as well, less shape alterations were seen in the sensorimotor striatum. The behavioral counterparts of these local shape changes in healthy individuals as well as in patients suffering from neurological and psychiatric disorders needs to be further explored. For example, it would be of interest to pinpoint the exact localization of striatal volume increase following antipsychotic drug treatment in patients with schizophrenia (Shenton et al., 2001), as these might be related to the clinical effects of these drugs.

Shape analysis is not intended to completely replace volume analysis. Volume analysis is simpler and faster to perform and, therefore, it should be used when reliable results are obtained. Shape analysis provides complementary information that may improve results in many cases. Shape analysis may be particularly useful for examining subtle structural deficits that do not manifest as volume loss of the whole structure. For example, schizophrenia is thought to be associated with subtle structural alterations reflecting abnormal neurodevelopment, and previous shape analyses have indeed demonstrated alterations in lateral ventricles (Styner et al., 2005), corpus callosum (Narr et al., 2002), and hippocampus (Csernansky et al., 1998; Tepest et al., 2003; Posener et al., 2003) in patients with schizophrenia. Defining the variation in striatal shape related to normal aging and gender will enhance future clinical studies in patient populations with this method.

Our future objectives include the combination of the shape analysis introduced in this paper with the functional information from the positron emission tomography (PET) images. Especially we will study how the changes in the anatomy correlate with the changes in the function of the brain: do the shape changes cause also changes in the function or vice versa?

Acknowledgments

Research was supported by TEKES Drug 2000 technology program and the Academy of Finland, project no. 213462 (Finnish Centre of Excellence program (2006–2011)).

References

Arun, K., Huang, T., Blostein, S., 1987. Least square fitting of two-point sets. IEEE Trans. Pattern Anal. Mach. Intell. 9 (5), 698–700.

Aylward, E., Sparks, B., Field, K., Yallapragada, V., Shpritz, B., Rosenblatt, A., Brandt, J., Gourley, L., Liang, K., Zhou, H., Margolis, R., Ross, C., 2004. Onset and rate of striatal atrophy in preclinical Huntington disease. Neurology 63 (1), 66–72.

Behrens, T., Johansen-Berg, H., Woolrich, M., Smith, S., Wheeler-Kingshott, C., Boulby, P., Barker, G., Sillery, E., Sheehan, K., Ciccarelli, O., Thompson, A., Brady, J., Matthews, P., 2003. Non-invasive mapping of connections between human thalamus and cortex using diffusion imaging. Nat. Neurosci. 6 (7), 750–757.

Bookstein, F., 1997. Shape and the information in medical images: a decade of the morphometric synthesis. Comput. Vis. Image Underst. 66 (2), 97–118.

Brabec, J., Krásenský, J., Petrovický, P., 2003. Volumetry of striatum and pallidum in man—Anatomy, cytoarchitecture, connections, MRI and aging. Sbor. lék. 104 (1), 13–65.

Brickman, A., Buchsbaum, M., Shihabuddin, L., Hazlett, E., Borod, J., Mohs, R., 2003. Striatal size, glucose metabolic rate, and verbal learning in normal aging. Cogn. Brain Res. 17 (1), 106–116.

Buchsbaum, M., Shihabuddin, L., Brickman, A., Miozzo, R., Prikryl, R., Shaw, R., Davis, K., 2003. Caudate and putamen volumes in good and poor outcome patients with schizophrenia. Schizophr. Res. 64 (1), 53–62.

Burke, S., Barnes, C., 2006. Neural plasticity in the ageing brain. Na. Rev., Neurosci. 7 (1), 30–40.

Christensen, G., Joshi, S., Miller, M., 1997. Volumetric transformation of brain anatomy. IEEE Trans. Med. Imag. 16 (6), 864–877.

Cootes, T., Taylor, C., Cooper, D., Graham, J., 1995. Active Shape Models—Their training and application. Comput. Vis. Image Underst. 61 (1), 38–59 (Jan.).

Csernansky, J., Joshi, S., Wang, L., Haller, J., Gado, M., Miller, J., Grenander, U., Miller, M., 1998. Hippocampal morphometry in schizophrenia by high dimensional brain mapping. Proc. Natl. Acad. Sci. U. S. A. 95 (19), 11406–11411.

Csernansky, J., Wang, L., Joshi, S., Ratnanather, J., Miller, M., 2004. Computational anatomy and neuropsychiatric disease: probabilistic assessment of variation and statistical inference of group difference, hemispheric asymmetry, and time-dependent change. NeuroImage 23, S56–S68.

Davatzikos, C., 1997. Spatial transformation and registration of brain images using elastically deformable models. Comput. Vis. Image Underst. 66 (2), 207–222.

Deshmukh, A., Rosenbloom, M., De Rosa, E., Sullivan, E., Pfefferbaum, A., 2005. Regional striatal volume abnormalities in schizophrenia: effects of comorbidity for alcoholism, recency of alcoholic drinking, and antipsychotic medication type. Schizophr. Res. 79 (2–3), 189–200.

Goldman-Rakic, P., 1996. Regional and cellular fractionation of working memory. Proc. Natl. Acad. Sci. U. S. A. 93 (24), 13473–13480.

Golland, P., Grimson, W., Shenton, M., Kikinis, R., 2005. Detection and analysis of statistical differences in anatomical shape. Med. Image Anal. 9 (1), 69–86.

Grady, C., 2000. Functional brain imaging and age-related changes in cognition. Biol. Psychol. 54 (1), 259–281.

Guillem, F., Mograss, M., 2005. Gender differences in memory processing: evidence from event-related potentials to faces. Brain Cogn. 57 (1), 84–92.

Gunduz, H., Wu, H., Ashtari, M., Bogerts, B., Crandall, D., Robinson, D., Alvir, J., Lieberman, J., Kane, J., Bilder, R., 2002. Basal ganglia volumes in first-episode schizophrenia and healthy comparison subjects. Biol. Psychiatry 51 (10), 801–808.

Gunning-Dixon, F., Head, D., McQuain, J., Acker, J., Raz, N., 1998. Differential aging of the human striatum: a prospective MR imaging study. Am. J. Neuroradiol. 19 (8), 1501–1507.

Gur, R., Gunning-Dixon, F., Turetsky, B., Bilker, W., Gur, R., 2002. Brain region and sex differences in age association with brain volume. Am. J. Geriatr. Psychiatry 10 (1), 72–80.

Haber, S., 2003. The primate basal ganglia: parallel and integrative networks. J. Chem. Neuroanat. 26 (4), 317–330.

Hollander, E., Anagnostou, E., Chaplin, W., Esposito, K., Haznedar, M., Licalzi, E., Wasserman, S., Soorya, L., Buchsbaum, M., 2005. Striatal volume on magnetic resonance imaging and repetitive behaviors in autism. Biol. Psychiatry 58 (3), 226–232.

Hwang, J., Lyoo, I., Dager, S., Friedman, S., Oh, J., Lee, J., Kim, S., Dunner, D., Renshaw, P., 2006. Basal ganglia shape alterations in bipolar disorder. Am. J. Psychiatry 163 (2), 276–285.

Lacerda, A., Nicoletti, M., Brambilla, P., Sassi, R., Mallinger, A., Frank, E., Kupfer, D., Keshavan, M., Soares, J., 2003. Anatomical MRI study of basal ganglia in major depressive disorder. Psychiatry Res. Neuroimaging 124 (3), 129–140.

Lee, J.-M., Kim, S., Jang, D., Ha, T., Kim, J.-J., Kim, I., Kwon, J., Kim, S., 2004. Deformable model with surface registration for hippocampal shape deformity analysis in schizophrenia. NeuroImage 22 (2), 831–840.

Levitt, J., McCarley, R., Dickey, C., Voglmaier, M., Niznikiewicz, M., Seidman, L., Hirayasu, Y., Ciszewski, A., Kikinis, R., Jolesz, F., Shenton, M., 2002. MRI study of caudate nucleus volume and its cognitive correlates in neuroleptic-naive patients with schizotypal personality disorder. Am. J. Psychiatry 159 (7), 1190–1197.

Levitt, J., Westin, C., Nestor, P., Estepar, R., Dickey, C., Voglmaier, M., Seidman, L., Kikinis, R., Jolesz, F., McCarley, R., Shenton, M., 2004. Shape of caudate nucleus and its cognitive correlates in neuroleptic-naive schizotypal personality disorder. Biol. Psychiatry 55 (2), 177–184.

Levy, R., Friedman, H., Davachi, L., Goldman-Rakic, P., 1997. Differential activation of the caudate nucleus in primates performing spatial and non-spatial working memory tasks. J. Neurosci. 17 (10), 3870–3882.

Lötjönen, J., 2003. Construction of patient-specific surface models from MR images: application to bioelectromagnetism. Comput. Methods Programs Biomed. 72 (2), 167–178.

Lötjönen, J., Reissman, P.-J., Magnin, I., Katila, T., 1999. Model extraction from magnetic resonance volume data using the deformable pyramid. Med. Image Anal. 3 (4), 387–406 (Dec.).

Manoach, D., Gollub, R., Benson, E., Searl, M., Goff, D., Halpern, E., Saper, C., Rauch, S., 2000. Schizophrenic subjects show aberrant fMRI activation of dorsolateral prefrontal cortex and basal ganglia during working memory performance. Biol. Psychiatry 48 (2), 99–109.

Narr, K., Cannon, T., Woods, R., Thompson, P., Kim, S., Asunction, D., van Erp, T., Poutanen, V., Huttunen, M., Lönnqvist, J., Standerksjöld-Nordenstam, C., Kaprio, J., Mazziotta, J., Toga, A., 2002. Genetic contributions to altered callosal morphology in schizophrenia. J. Neurosci. 22 (9), 3720–3729.

Parent, A., Hazrati, L., 1995. Functional-anatomy of the basal ganglia. I. The Cortico-Basal Ganglia-Thalamo-Cortical Loop. Brain Res. Rev. 20 (1), 91–127.

Posener, J., Wang, L., Price, J., Gado, M., Province, M., Miller, M., Babb, C., Csernansky, J., 2003. High-dimensional mapping of the hippocampus in depression. Am. J. Psychiatry 160 (1), 83–89.

Press, W., Teukolsky, S., Vetterling, W., Flannery, B., 1992. Numerical recipes in C: the art of scientific computing, 2nd Edition. Cambridge Univ. Press.

Rilea, S., Roskos-Ewoldsen, B., 2004. Sex differences in spatial ability: a lateralization of function approach. Brain Cogn. 56 (3), 332–343.

Rueckert, D., Sonoda, L., Hill, D., Leach, M., Hawkes, D., 1999. Nonrigid registration using free-form deformations: application to breast MR images. IEEE Trans. Med. Imag. 18 (8), 712–721 (Aug.).

Sampath, Y., Vetsa, K., Styner, M., Pizer, S., Lieberman, J., Gerig, G., 2003. Caudate shape discrimination in schizophrenia using template-free non-parametric tests. Medical Image Computing and Computer-Assisted Intervention (MICCAI'03). Montréal, Canada, pp. 661–669.

Sederberg, T., Parry, S., 1986. Free-form deformation of solid geometric models. Proc. International Conference on Computer Graphics and Interactive Techniques (SIGGRAPH'86). Dallas, USA, pp. 151–160.

Shenton, M., Dickey, C., Frumin, F., McCarley, R., 2001. A review of MRI findings in schizophrenia. Schizophr. Res. 49 (1), 1–52.

Shihabuddin, L., Buchsbaum, M., Hazlett, E., Silverman, J., New, A., Brickman, A., Mitropoulou, V., Nunn, M., Fleischman, M., Tang, C., Siever, L., 2001. Striatal size and relative glucose metabolic rate in schizotypal personality disorder and schizophrenia. Arch. Gen. Psychiatry 58 (9), 877–884.

Strakowski, S., DelBello, M., Zimmerman, M., Getz, G., Mills, N., Ret, J., Shear, P., Adler, C., 2002. Ventricular and periventricular structural volumes in first-versus multiple-episode bipolar disorder. Am. J. Psychiatry 159, 1841–1847.

Styner, M., Lieberman, J., Pantazis, D., Gerig, G., 2004. Boundary and medial shape analysis of the hippocampus in schizophrenia. Med. Image Anal. 8 (3), 197–203.

Styner, M., Lieberman, J., McClure, R., Weinberger, D., Jones, D., 2005. Morphometric analysis of lateral ventricles in schizophrenia and healthy controls regarding genetic and disease-specific factors. Proc. Natl. Acad. U. S. A. 102 (13), 4872–4877.

Szabo, C., Lancaster, J., Xiong, J., Cook, C., Fox, P., 2003. MR imaging volumetry of subcortical structures and cerebellar hemispheres in normal persons. Am. J. Neuroradiol. 24 (4), 644–647.

Tepest, R., Wang, L., MIller, M., Falkai, P., Csernansky, J., 2003. Hippocampal deformities in the unaffected siblings of schizophrenia subjects. Biol. Psychiatry 54 (11), 1234–1240.

Thompson, P., Toga, A., 2002. A framework for computational anatomy. Comput. Vis. Sci. 5 (1), 13–34.

Uitenbroek, D., 1997. SISA-Binomial. Available: http://home.clara.net/sisa/binomial.htm. (Accessed: 2005, August 24).

Xu, J., Kobayashi, S., Yamaguchi, S., Iijima, K., Okada, K., Yamashita, K., 2000. Gender effects on age-related changes in brain structure. Am. J. Neuroradiol. 21 (1), 112–118.